Spectrochimica Acta Part A: Molecular and Biomolecular Spectroscopy 252 (2021) 119502

Contents lists available at ScienceDirect

Spectrochimica Acta Part A: Molecular and Biomolecular Spectroscopy

journal homepage: www.elsevier.com/locate/saa

A resorufin-based red-emitting fluorescent probe with high selectivity for tracking endogenous peroxynitrite in living cells and inflammatory mice

Huihui Su [a,1], Nannan Wang [a,1], Jiamin Wang [b,*], Han Wang [a], Jian Zhang [a,*], Weili Zhao [a,*]

[a] Key Laboratory for Special Functional Materials of Ministry of Education, School of Materials Science and Engineering, Henan University, Kaifeng 475004, PR China
[b] Key Laboratory of Natural Medicine and Immuno-Engineering of Henan Province, Henan University, Kaifeng 475004, PR China

HIGHLIGHTS

- A novel Resorufin-based fluorescent probe for selective detection of $ONOO^-$ were developed.
- Probe displayed high selectivity towards to $ONOO^-$.
- Probe could sense intracellular $ONOO^-$ by fluorescent imaging in living cells and inflammatory mice.

GRAPHICAL ABSTRACT

In this work, a new resorufin-based turn-on fluorescent probe (**RFP**) carrying phosphinate recognition group [$-P(O)Ph_2$] as a good trigger group was designed and synthesized. The probe exhibited highly selectivity and sensitivity for detecting endogenous $ONOO^-$ in RAW264.7 cells and inflammatory mice.

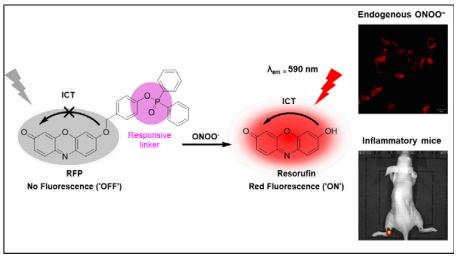

ARTICLE INFO

Article history:
Received 10 December 2020
Received in revised form 11 January 2021
Accepted 14 January 2021
Available online 30 January 2021

Keywords:
Peroxynitrite
Resorufin
Red-emitting fluorescent probe
Live cell imaging
Inflammatory mice imaging

ABSTRACT

Peroxynitrite ($ONOO^-$) plays essential roles on various physiological and pathological processes of living systems as a short-lived and highly reactive nitrogen (RNS) specie. The construction of novel long-wavelength fluorescent probes with high specificity towards $ONOO^-$ for imaging in *vivo* is still demand urgently. About this work, a novel resorufin-based red-emitting fluorescent probe for tracking $ONOO^-$ has been constructed. The probe **RFP** exhibited high selectivity towards $ONOO^-$ anion over other analytes. Utilizing the probe, $ONOO^-$ could be directly observed by the naked eye. Furthermore, **RFP** was successfully applied for imaging endogenous $ONOO^-$ in RAW264.7 cells and inflammatory mice. This work offers a convenient method for monitoring the intercellur $ONOO^-$ that be expected to be applied for explaining the bio-functional roles of $ONOO^-$ in living system.

1. Introduction

As a short-lived and highly reactive nitrogen (RNS) specie, peroxynitrite ($ONOO^-$) plays essential roles on various physiological and pathological processes of living systems [1]. It is generated through the diffusion control chemical transformation reaction of nitric oxide (NO) and superoxide ($O_2^{\cdot-}$) [2]. Peroxynitrite is a potent cytotoxic substance which could react with large numbers of biological species including nucleic acids, lipids and proteins, eventually result in apoptosis [3]. Furthermore, it is not negligible that peroxynitrite is a stronger oxidizer than NO or $O_2^{\cdot-}$. Until now, mounting evidences suggested that excessive $ONOO^-$ could cause many diseases, such as inflammatory, neurodegenerative, Alzhei-

* Corresponding authors.
E-mail addresses: jmwang@henu.edu.cn (J. Wang), jianzhang@henu.edu.cn (J. Zhang), zhaow@henu.edu.cn (W. Zhao).
[1] These authors contributed equally.

https://doi.org/10.1016/j.saa.2021.119502
1386-1425/

mer's disease, Parkinson's disease, cardiovascular, ischemic reperfusion injury and cancer [4–7]. Thus, it is vitally necessary to build up a new method for detecting cellular $ONOO^-$ and explore its role in disease diagnosis and various pathophysiological properties.

To date, fluorescent analytical method is one of the most useful tools for widely applying in chemical analysis, bioanalysis, and medicine study owing to its outstanding advantages of rapid response, real-time visualization, excellent sensitivity and noninvasive nature [8–13]. Recently, numerous fluorescent probes for tracing $ONOO^-$ in living cells have been reported [14–27]. These chemical reaction-based probes could be roughly divided into several mechanisms: oxidation of boronate [28,29], oxidation of phosphyl/phosphinate [30–34], oxidation of ketones [35], redox reactions of selenium [36], oxidative N-dearylation [37,38] and other reaction strategies. Although the reported probes are executed well to monitor $ONOO^-$, there still exist some limitations, like low selectivity (some $ONOO^-$ probes could respond to H_2O_2 and NaClO as well) [39,40] and absorption/ emission in the short-wavelength, which probable unavoidably interfered by biological autofluorescence and enslaved to shallow tissue penetration [41,42]. Moreover, the study on $ONOO^-$ fluorescent probes in inflammatory model is none the less limited so far [43–45]. Therefore, the construction of novel long-wavelength fluorescent probes with high specificity towards $ONOO^-$ is still urgently demand.

Our group has committed to designing and synthesizing fluorescent sensors for various reactive species [46–51]. Fortunately, the fluorescent probes we developed have excellent selectivity and sensitivity. Take the advantage of good water solubility and long-wavelength, resorufin was chosen as the fluorophore. Besides, alkylation of the 7-hydroxy group of resorufin could induce efficient fluorescence quenching [52–59]. Based on functional diphenyl phosphinate recognition group [60], we designed and synthesized a resorufin-based red-emitting "turn-on" fluorescent probe **RFP** of $ONOO^-$ detection (Scheme 1). We have demonstrated the practical utility of **RFP** in chemical and biological circumstance. Probe **RFP** showed highly selectivity towards $ONOO^-$, particularly over NaClO and H_2O_2. To our delight, this probe could trace $ONOO^-$ by naked-eye. Importantly, **RFP** enabled the direct image endogenous $ONOO^-$ in both living cells and inflammatory mice.

2. Experimental

2.1. Reagents and instruments

All solvents and chemicals were purchased online without further purification. The ^1H NMR and ^{13}C NMR spectra were performed on a Bruker AVANCE NEO 500 instrument. UV–vis spectra were obtained by using a PE Lambda 950 UV–vis spectrometer. Fluorescence spectra were recorded using JY HORIBA FluoroLog-3 spectra fluorophotometer. High resolution mass spectra were obtained by using Bruke solanX 70 FT-MS spectra.

2.2. Cell culture and cell imaging

RAW264.7 cells were pretreated with LPS and IFN-γ for 12 h and then the probe **RFP** (10 μM) was added to RAW264.7 cells and incubated for another 30 min then washed by PBS twice. For the control experiment, RAW264.7 cells with treatment of **RFP** (10 μM) for 30 min. The fluorescence images of cells were obtained by Laser scanning confocal microscopy (Ziss 880) (λ_{ex} = 561 nm).

2.3. Fluorescence imaging in inflammatory mice

All animal care and experimental protocols for this study were approved by the Animal Experiment Ethics Committee of Henan University. To experimental groups, the nude mice were subcutaneously injected with a volume of 200 μL LPS for 12 h in left leg to cause inflammation, then following subcutaneous injection with **RFP** (500 μM, 200 μL) in situ. For the control group, the nude mice were injected with same volume of 200 μL saline for 12 h in the right leg then following subcutaneous injection of **RFP** in situ. Using the fluorescence imaging system (VISQUE In Vivo Elite) to gain the whole-body imaging.

3. Results and discussions

3.1. Spectral properties of *RFP* towards $ONOO^-$

The fluorescent probe **RFP** was obtained by three steps (Scheme S1). The compounds were characterized by HR-MS, ^1H NMR, and ^{13}C NMR (supporting information). The probe consisted of three parts, resorufin moiety as fluorophore, diphenyl phosphate group as the specific triggered part reacting with $ONOO^-$ and benzyl ether as the self-immolation linker which enabled quench the fluorescence of the resorufin. We firstly investigated the spectral properties of **RFP** in the absence and presence of $ONOO^-$ in PBS buffer (10 mM, pH 7.4, containing 1% DMSO, 3 mM Hexadecyl trimethyl ammonium Bromide, CTAB) at 37 ℃. As shown in Fig. 1, the maximum absorption peak of **RFP** itself was at 469 nm with negligible fluorescence intensity at 590 nm. After treatment with $ONOO^-$, the maximum absorption band showed a red-shift from 469 to 585 nm. Besides, as shown in Fig. 1b, its fluorescence intensity at 590 nm was increased almost 25-fold. Apart from dramatic fluorescence intensity increased by adding $ONOO^-$, the color of solution remarkably changed from yellow to pink, this change could be directly observed by the naked eye. These results confirmed that the fluorescent probe **RFP** was available to detect $ONOO^-$.

Additionally, we measured the fluorescence enhancement in different durations. As shown in Fig. 2a, after reacting with $ONOO^-$, the maximum absorption at 469 nm was gradually decreased and increased at 585 nm within 20 min. Besides, the fluorescence intensity at 590 nm increased rapidly within 10 min, however, gradually and finally stabilized at 20 min (Fig. 2b), which indicated that the process of self-elimination was finished in 20 min. Inset in the Fig. 2b more clearly showed the kinetic curve of fluorescence intensity for **RFP** at 590 nm in the presence of $ONOO^-$ at different times.

Furthermore, the fluorescence titration assay was performed, the fluorescence responses over the concertation of 0–100 μM $ONOO^-$ with **RFP** were obtained, Fig. 3a was clearly demonstrated that the fluorescence intensity of **RF**P increased in a $ONOO^-$ dose-dependent manner. Simultaneously, a good linear relationship between the fluorescence intensity and $ONOO^-$ concentration from 0 to 35 μM was obtained (Fig. 3b), and the detection limit was calculated to be 238 nM based on 3σ/k, detection limit implied the possibility of accurate measurement in vitro testing.

3.2. Selectivity of *RFP*

A successful fluorescent probe for applicating with biological samples should bear some advantages including high selectivity, high sensitivity and high resolution. Due to the biological system often contains other ROSs/RNSs, the selectivity of the probe **RFP** towards $ONOO^-$ were following investigated, including various ROSs: ($O_2^{\cdot -}$; $^1O_2$; $^{\cdot}OH$; O^tBu; H_2O_2; OCl^-,), amino acids (Cys; Hcy; GSH), ions (K^+; Na^+; Ca^+), and other analyte (H_2S; HSO_3^-; SO_4^{2-}; SO_3^{2-}; CO_3^{2-}; HCO_3^-; NO_2^-; NO). According to the experimental results (Fig. 4a), it can be clearly observed that among all of the analyte, only $ONOO^-$ could trigger the remarkable fluorescent intensity

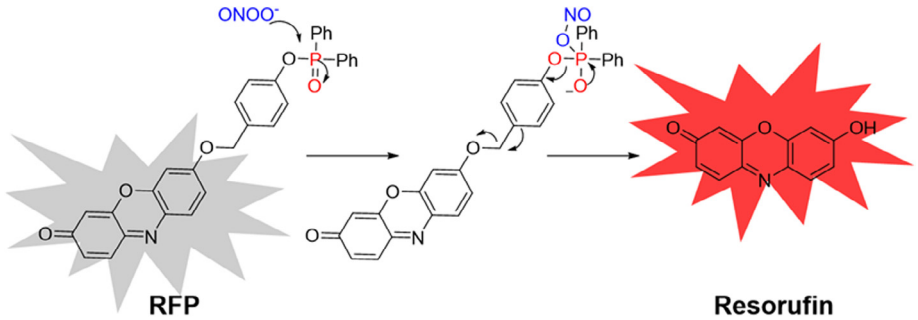

Scheme 1. Proposed recognition mechanism of **RFP** toward $ONOO^-$.

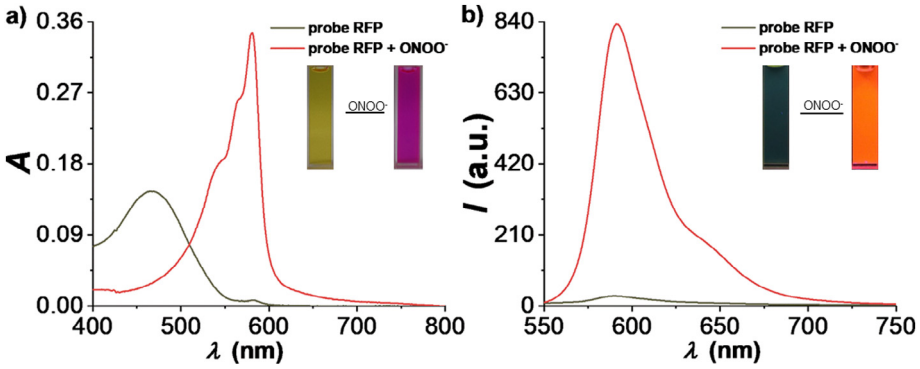

Fig. 1. (a) UV–vis spectra and (b) fluorescence changes of probe **RFP** in absence and presence of $ONOO^-$. The probe was incubated in PBS (pH 7.4, 10 mM, 1% DMSO, 3 mM CTAB) at 37 ℃ for 30 min. Inset of (a): The colour change of **RFP** in the absence and presence of $ONOO^-$ under daylight. (b) photography of **RFP** in the absence (right) and presence (left) of $ONOO^-$ at 365 nm, λ_{ex} = 525 nm.

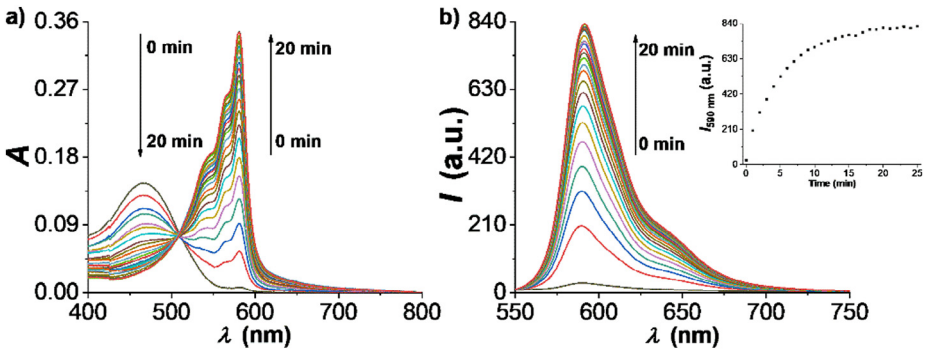

Fig. 2. (a) Time-dependent absorption and (b) fluorescence spectra of **RFP** (10 μM) towards to $ONOO^-$ (100 μM). The probes were incubated at 37 ℃ in PBS (pH 7.4, 10 mM, 1% DMSO, 3 mM CTAB). inset: Scatter plot of the time-dependent curve: the probe and $ONOO^-$ react completely within 20 min, λ_{ex} = 525 nm.

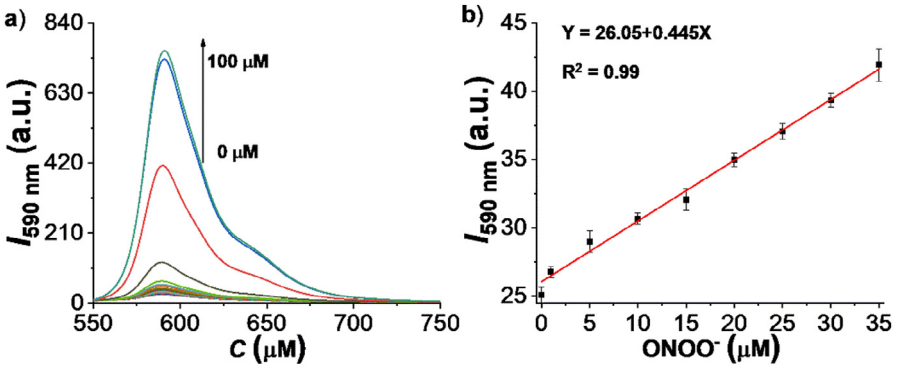

Fig. 3. (a) Fluorescence titration of **RFP** with $ONOO^-$. (b) Changes in fluorescence intensity of RFP at 590 nm as a function of [$ONOO^-$]. **RFP** (10 μm) and $ONOO^-$ (0–35 μm) in PBS (pH 7.4, 10 mM, 1% DMSO, 3 mM CTAB, λ_{ex} = 525 nm).

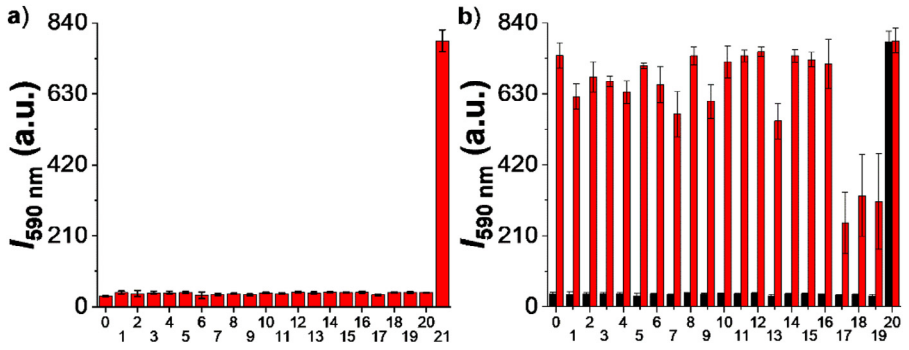

Fig. 4. Fluorescence intensity response of **RFP** (10 μM) at 590 nm by treating with various biological species. (a) 0:blank, 1: $O_2^{\cdot -}$, 2: $^1O_2$, 3:OH, 4:O^{t}Bu, 5: H_2O_2, 6: OCl^-, 7: H_2S, 8: HSO_3^-, 9: SO_4^{2-}, 10: SO_3^{2-}, 11: CO_3^{2-}, 12: HCO_3^-, 13: NO_2^-, 14: NO, 15: K^+, 16: Na^+, 17: Ca^+,18: Cys, 19: Hcy, 20: GSH, 21: $ONOO^-$. (b) 0:$O_2^{\cdot -}$, 1:$^1O_2$, 2:OH, 3:O^{t}Bu, 4:H_2O_2, 5: OCl^-, 6: H_2S, 7:HSO_3^-, 8:SO_4^{2-}, 9:SO_3^{2-}, 10:CO_3^{2-}, 11:HCO_3^-, 12:NO_2^-, 13:NO, 14:K^+, 15:Na^+, 16:Ca^+, 17:Cys, 18:Hcy, 19:GSH, and 20:$ONOO^-$ All analytes were kept at a final concentration of 100 μM and the mixture solution were incubated at 37 ℃ in PBS (pH 7.4, 10 mM, 1% DMSO, 3 mM CTAB) for 30 min in advance, λ_{ex} = 525 nm and λ_{em} = 590 nm.

change in 590 nm. In addition, we compared the superoxide anions from different sources, and found that **RFP** had no response (Figure S2). Anti-interference ability is an essential indicator of a probe, in line with our expectations, the probe **RFP** could enable to respond to $ONOO^-$ with similar degrees of fluorescence enhancement even in the presence of other related species (Fig. 4b). It is noteworthy that intracellular thiols (such as GSH, Hcy, Cys) were the central of reducing sources to cellular redox homeostasis [61], especially GSH was the most abundant endogenous thiol. Even if excessive thiols exist, the probe **RFP** could still respond to $ONOO^-$ with significant fluorescence enhancement. These results suggested its potential applicability of tracking $ONOO^-$ in complex biological environment.

3.3. Effect of pH

With this high selectivity fluorescent probe in hand, its pH stability towards the $ONOO^-$ were investigated, in different pH value from 6.0 to 8.0, the probe **RFP** itself was so stable that almost no fluorescent (Figure S1) when incubated in 37 ℃ for 1 h. On the contrast, it showed obviously fluorescent intensity enhancement in the presence of $ONOO^-$ in different pH value from 6.0 to 8.0, which implied potential application in biological samples to detect $ONOO^-$. Therefore, we speculated that the probe **RFP** was stable and could detect $ONOO^-$ in the physiological environment.

In addition, we listed several types of representative probes based on functional diphenyl phosphinate recognition group for $ONOO^-$ sensing reported to date (Table 1). We compared the sensing performance in terms of the saturation time, linear range and sensitivity of the RFP with other works. Although the performance of our works is not optimal, but on the whole, the RFP in our work showed faster response time and lower detection limit.

3.4. Study on the sensing mechanism

A briefly description for the working mechanism of the fluorescent probe as followed (the reaction mechanism was shown in Scheme 1), in the presence of $ONOO^-$ which could attack the triggered moiety, the diphenyl phosphate group was cleaved and then underwent a step of self-elimination, finally the resorufin with red fluorescence was exposed. To certify the response mechanism, the product of the reaction of **RFP** with $ONOO^-$ was recorded by MS, from Figure S2, the major peak of the product found at m/z = 212.50 $[M-H]^-$ was consistent with the anion mode of the fluorophore, which supported the proposed mechanism.

To gain a clearer explanation about the photophysical properties of **RFP** in the presence of $ONOO^-$, theoretical calculations were conducted by density functional theory (DFT) with the mGGA / MII-L method basis set through the Materials Studio. The optimized geometries and the highest occupied molecular orbitals

Table 1
Performance comparison with other $ONOO^-$ sensors.

NO.	Sensors	$\lambda_{ex}/\lambda_{em}$ (nm)	buffer solution (v/v)	Saturation time (min)	Liner range (μM)	Detection limit (nM)	Ref.
1	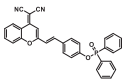	555/690↑ (~120-fold)	DMSO : PBS = 1 : 1	20	0 ~ 150	4620	[33]
2	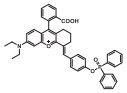	670/742↑ (~10-fold)	DMSO : PBS = 1 : 1	40	0 ~ 40	400	[30]
3	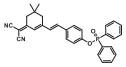	527/665↑ (~100-fold)	DMSO : PBS = 1 : 1	20	0 ~ 10	33	[31]
4	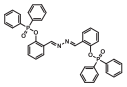	403/520↑ (~12-fold)	DMSO : PBS = 1 : 99	18	0 ~ 45	80	[42]
5	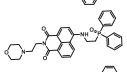	445/532↓ (~10-fold)	DMSO : PBS = 1 : 9	0.25	0 ~ 80	17.6	[32]
6	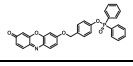	525/590↑ (~25-fold)	DMSO : PBS = 1 : 99 (3 mM CTAB)	20	0 ~ 35	238	This work

(HOMO) and lowest unoccupied molecular orbitals (LUMO) of the probe and resorufin were clearly showed in Fig. 5. For the probe **RFP**, both the LUMO and HOMO π-electrons of probe were mainly located on phenoxazine moiety, the intramolecular charge transfer (ICT) process was prevented due to the protection of hydroxy by diphenyl phosphinate. The HOMO π-electrons of resorufin were located on the whole molecular, while LUMO π-electrons resorufin were mainly distributed in the carbonyl moiety, the ICT progress was recovered. Besides, the HOMO and LOMO energy level of probe were −6.012 eV and −3.880 eV respectively, the energy gap (ΔE) was 2.132 eV. After reacting with $ONOO^-$, the HOMO and LOMO energy level of resorufin were changed to −5.417 eV and −3.546 eV respectively, the energy gap was narrowed to 1.871 eV. In this respect, the HOMO-LUMO energy gap tended to narrow which was consistent with the obvious red shift in the absorption spectrum of probe **RFP**. The theory calculations were in good accordance with the experimental results that rationalized the ICT process.

3.5. Live cell imaging

We first investigated the biocompatibility, since the prerequisite of a probe to cell and in vivo imaging was biocompatibility. The cytotoxic effects of **RFP** on cells were performed by the CCK-8 assays (Figure S3), **RFP** showed low cytotoxicity at concentrations up to 20 μM in live cells, laying a good foundation for biological application. We then examined the potential of **RFP** for visualizing $ONOO^-$ in RAW264.7 cells. It was known that

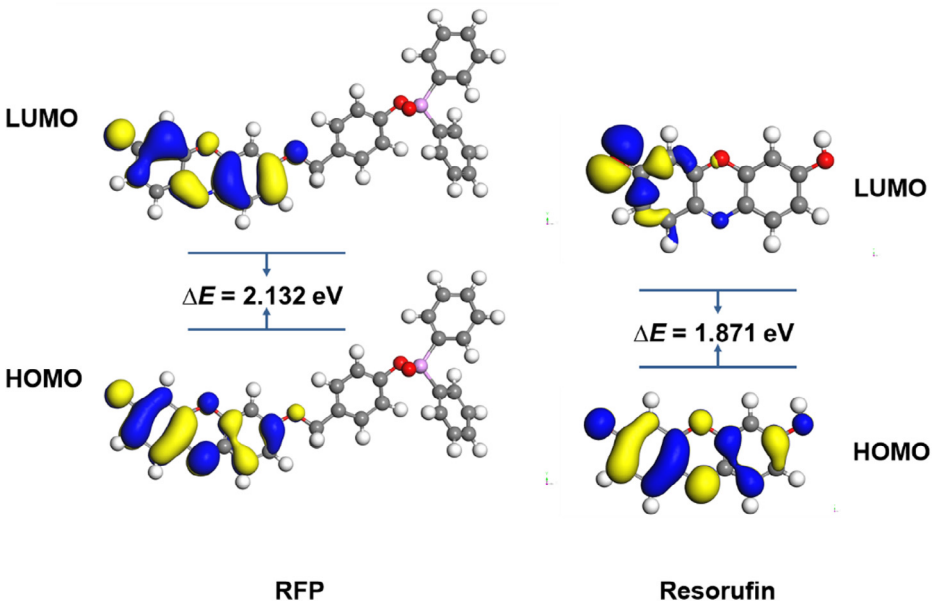

Fig. 5. Molecular orbital plots and the corresponding HOMO and LUMO energy gaps of **RFP** before and after reacting with $ONOO^-$.

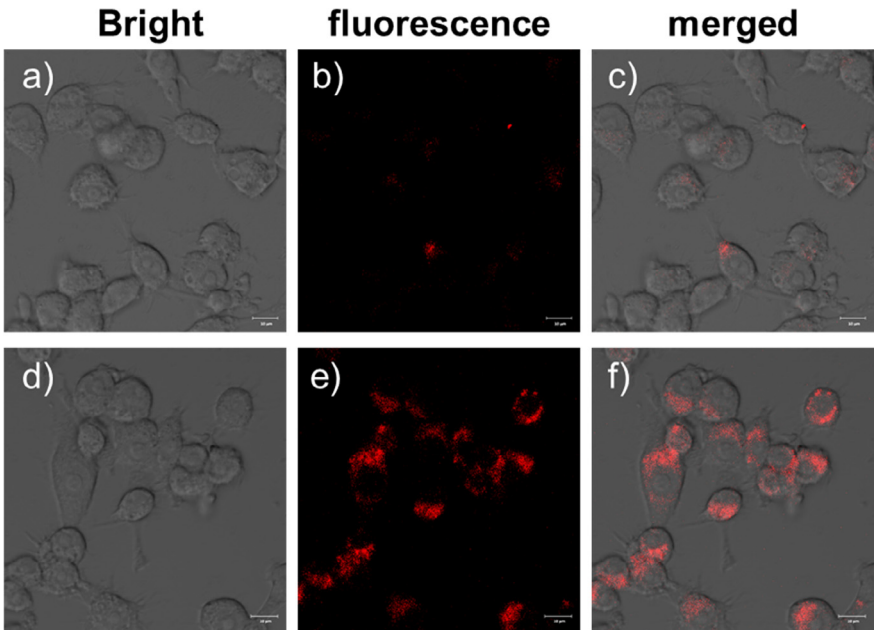

Fig. 6. (a) Bright filed and (b) fluorescence images of RAW264.7 cells treated with 10 μM **RFP** for 30 min and (d) bright filed and (e) fluorescence images of RAW264.7 cells by preincubation with LPS and INF-γ for 12 h followed treated with 10 μM **RFP** for 30 min. (c) was the overlap of (a) and (b); (f) was the overlap of (d) and (e).

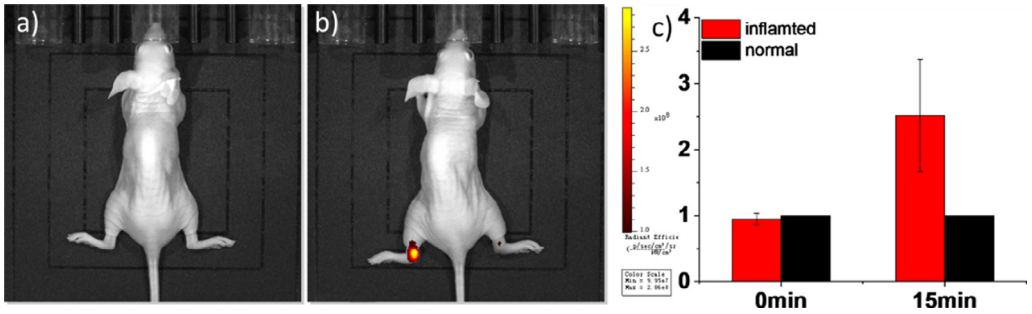

Fig. 7. Fluorescent imaging of mice at 0 min (a) and 15 min (b). The left leg of mice was subcutaneously injected with LPS (1 mg/mL, 200 μL) for causing inflammation and the right leg was subcutaneously injected the same volume of saline as a blank control. After 12 h, the **RFP** (50 μL, 500 μM, DMSO/saline = 1/9) was subcutaneously injected in situ. (c) Relative fluorescent intensity from the normal and inflamed tissues. All assays were performed in triplicate and expressed as the mean ± SD.

RAW264.7 cells could produce $ONOO^-$ by stimulating with lipopolysaccharide (LPS) and pro-inflammatory cytokine interferon-gamma (IFN-γ) [37]. As illustrated in Fig. 6, after only incubated with **RFP**, the RAW264.7 cells exhibited weak red fluorescence. As expected, the cells incubated with LPS and INF-γ displayed obviously red fluorescence. These results demonstrated that the probe **RFP** could track the endogenous $ONOO^-$ in the living cells.

3.6. Inflammatory mice imaging

According to the previous literature [62], LPS was used to induce inflammation in nude mice in this study (Fig. 7). The left leg of mice was subcutaneously injected with LPS (1 mg/mL, 200 μL) for causing inflammation and the right leg was subcutaneously injected the same volume of saline as a blank control. After 12 h, the **RFP** was subcutaneously injected in situ incubated for 30 min. Compared with normal tissues, the LPS-stimulated inflammation tissues were clearly showed an obviously enhancement of fluorescence intensity, as expected. Moreover, the fluorescence intensity reached the maximum in 15 min indicating that **RFP** could quickly track endogenous $ONOO^-$ in inflamed mice in situ.

4. Conclusions

In summary, we reported a new red-emitting fluorescent probe for tracking $ONOO^-$ based on resorufin. The probe **RFP** exhibited high selectivity towards $ONOO^-$ anion over other analytes. Utilizing the probe, $ONOO^-$ could be directly observed by the naked eye. Furthermore, we successfully applied **RFP** for imaging endogenous $ONOO^-$ in living RAW264.7 cells and inflamed mice. With these results, we envisioned that the probe **RFP** may have a promising prospect to be applied for elucidating the biofunctional roles of $ONOO^-$ in living system.

CRediT authorship contribution statement

Huihui Su: Methodology, Formal analysis, Writing - original draft. **Nannan Wang:** Data curation, Writing - original draft. **Jiamin Wang:** Conceptualization, Project administration, Writing - review & editing. **Han Wang:** Visualization. **Jian Zhang:** Writing - review & editing, Resources. **Weili Zhao:** Writing - review & editing, Resources.

Declaration of Competing Interest

The authors declare no competing financial interest.

Acknowledgements

We gratefully acknowledge financial support from the National Natural Science Foundation of China (no. 21372063, no. 21702046), the China Postdoctoral Science Foundation (no. 2018 M632757), Innovation Scientists and Technicians Troop Construction Projects of Henan Province (no. 20IRTSTHN020). The authors thank Prof. Changwei Gong, School of Materials Science and Technology, Taiyuan University of Science and Technology, for his helpful discussions on the density functional theory calculations.

Appendix A. Supplementary data

Supplementary data to this article can be found online at https://doi.org/10.1016/j.saa.2021.119502.

References

[1] C. Nathan, A. Cunningham-Bussel, Beyond oxidative stress: an immunologist's guide to reactive oxygen species, Nat. Rev. Immunol. 13 (2013) 349–361.
[2] R. Radi, Peroxynitrite, a stealthy biological oxidant, J. Biol. Chem. 288 (2013) 26464–26472.
[3] G. Ferrer-Sueta, R. Radi, Chemical biology of peroxynitrite: kinetics, diffusion, and radicals, ACS Chem. Biol. 4 (2009) 161–177.
[4] H. Li, X. Li, X. Wu, W. Shi, H. Ma, Observation of the generation of $ONOO^-$ in mitochondria under various stimuli with a sensitive fluorescence probe, Anal. Chem. 89 (2017) 5519–5525.
[5] T. Nagano, J. Clin, Bioimaging probes for reactive oxygen species and reactive nitrogen species, Biochem. Nutr. 45 (2009) 111–124.
[6] Z. Chen, Z. Tian, K. Kallio, A.L. Oleson, A. Ji, D. Borchardt, D. Jiang, S.J. Remington, H. Ai, The N-B interaction through a water bridge: understanding the chemoselectivity of a fluorescent protein based probe for peroxynitrite, J. Am. Chem. Soc. 138 (2016) 4900–4907.
[7] A.C. Sedgwick, H. Han, J.E. Gardiner, S.D. Bull, X. He, T.D. James, The development of a novel AND logic based fluorescence probe for the detection of peroxynitrite and GSH, Chem. Sci. 9 (2018) 3672–3676.
[8] H. Li, W. Shi, X. Li, Y. Hu, Y. Fang, H. Ma, Ferroptosis accompanied by •OH generation and cytoplasmic viscosity increase revealed via dual-functional fluorescence probe, J. Am. Chem. Soc. 141 (2019) 18301–18307.
[9] X. Li, X. Gao, W. Shi, H. Ma, Design strategies for water-soluble small molecular chromogenic and fluorogenic probes, Chem. Rev. 114 (2014) 590–659.
[10] Y. Huang, Y. Zhang, F. Huo, J. Chao, F. Cheng, C. Yin, A new strategy: distinguishable multi-substance detection, multiple pathway tracing based on a new site constructed by the reaction process and its tumor targeting, J. Am. Chem. Soc. 142 (2020) 18706–18714.
[11] H. Li, Y. Liu, X. Li, X. Li, H. Ma, Design, synthesis and application of a dual-functional fluorescent probe for reactive oxygen species and viscosity, Spectrochim. Acta Part A Mol. Biomol. Spectrosc. 246 (2021), 119059.
[12] Q. Gong, W. Shi, L. Li, X. Wu, H. Ma, Ultrasensitive fluorescent probes reveal an adverse action of dipeptide peptidase IV and fibroblast activation protein during proliferation of cancer cells, Anal. Chem. 88 (2016) 8309–8314.
[13] Q. Gong, W. Shi, L. Li, H. Ma, Leucine aminopeptidase may contribute to the intrinsic resistance of cancer cells toward cisplatin as revealed by an ultrasensitive fluorescent probe, Chem. Sci. 7 (2016) 788–792.
[14] D. Cheng, J. Peng, Y. Lv, D. Su, D. Liu, M. Chen, L. Yuan, X. Zhang, De Novo design of chemical stability near-infrared molecular probes for high-fidelity hepatotoxicity evaluation in vivo, J. Am. Chem. Soc. 141 (2019) 6352–6361.

[15] L.C. Murfin, M. Weber, S.-J. Park, W.-T. Kim, C.M. Lopez-Alled, C.L. McMullin, F. Pradaux-Caggiano, C.L. Lyall, G. Kociok-Köhn, J. Wenk, S.D. Bull, J. Yoon, H.-M. Kim, T.D. James, S.E. Lewis, Azulene-Derived fluorescent probe for bioimaging: detection of reactive oxygen and nitrogen species by two-photon microscopy, J. Am. Chem. Soc. 141 (2019) 19389–19396.
[16] S. Wang, L. Chen, P. Jangili, A. Sharma, W. Li, J.-T. Hou, C. Qin, J. Yoon, J.-S. Kim, Design and applications of fluorescent detectors for peroxynitrite, Coordin. Chem. Rev. 374 (2018) 36–54.
[17] W. Shu, Y. Wu, S. Zang, S. Su, H. Kang, J. Jing, X. Zhang, A mitochondria-targeting highly specific fluorescent probe for fast sensing of endogenous peroxynitrite in living cells, Sens. Actuators, B 303 (2020), 127284.
[18] D. Li, S. Wang, Z. Lei, C. Sun, A.M. El-Toni, M.S. Alhoshan, Y. Fan, F. Zhang, Peroxynitrite activatable NIR-II fluorescent molecular probe for drug-induced hepatotoxicity monitoring, Anal. Chem. 91 (2019) 4771–4779.
[19] Q. Sun, J. Xu, C. Ji, M.S. Shaibani, Z. Li, K. Lim, C. Zhang, L. Li, Z. Liu, Ultrafast detection of peroxynitrite in parkinson's disease models using a near-infrared fluorescent probe, Anal. Chem. 92 (2020) 4038–4045.
[20] G. Wang, Y. Wang, C. Wang, C. Huang, N. Jia, A new long-wavelength fluorescent probe for tracking peroxynitrite in live cells and inflammatory sites of zebrafish, Analyst 145 (2020) 828–835.
[21] J.-T. Hou, B. Wang, Y. Zhang, B. Cui, X. Cao, M. Zhang, Y. Ye, S. Wang, Observation of peroxynitrite overproduction in cells during 5-fluorouracil treatment via ratiometric fluorescent probe, Chem. Commun. 56 (2020) 2759–2762.
[22] C. Liu, Q. Duan, Z. Xue Zhang, P. Li, H. Jia, Y. Zhu, Z. Yu, B. Wang, W.S. Zhu, A novel hepatoma-specific fluorescent probe for imaging endogenous peroxynitrite in live HepG2 cells, Sens. Actuators, B 289 (2019) 124–130.
[23] X. Yin, W. Feng, S. Gong, G. Feng, Near-infrared fluorescent probe with rapid response and large Stokes shift for imaging peroxynitrite in living cells, zebrafish and mice, Dyes Pigments 172 (2020), 107820.
[24] G. Lu, Y. Guo, J. Zhuo, X. Li, H. Chi, Z. Zhang, A general strategy for through-bond energy transfer fluorescence probes combining intramolecular charge transfer: a silyl ether system for endogenous peroxynitrite sensing, Chem. Eur. J. 25 (2019) 16350–16357.
[25] J. Xiong, W. Wang, C. Wang, C. Zhong, R. Ruan, Z. Mao, Z. Liu, Visualizing peroxynitrite in microvessels of the brain with stroke using an engineered highly specific fluorescent probe, ACS Sens. 5 (2020) 3237–3245.
[26] Z. Wang, F. Zhang, J. Xiong, Z. Mao, Z. Liu, Investigations of drug-induced liver injury by a peroxynitrote activatable two-photon fluorescence probe, Spectrochim. Acta Part A Mol. Biomol. Spectrosc. 246 (2021), 118960.
[27] M. Li, H. Han, H. Zhang, S. Song, S. Shuang, C. Dong, Boronate based sensitive fluorescent probe for the detection of endogenous peroxynitrite in living cells, Spectrochim. Acta Part A Mol. Biomol. Spectrosc. 243 (2021), 118683.
[28] A. Sikora, J. Zielonka, M. Lopez, J. Joseph, B. Kalyanaraman, Direct oxidation of boronates by peroxynitrite: mechanism and implications in fluorescence imaging of peroxynitrite, Free Radical Biol. Med. 47 (2009) 1401–1407.
[29] X. Sun, Q. Xu, G. Kim, S.E. Flower, J.P. Lowe, J. Yoon, J.S. Fossey, X. Qian, S.D. Bull, T.D. James, A water-soluble boronate-based fluorescent probe for the selective detection of peroxynitrite and imaging in living cells, Chem. Sci. 5 (2014) 3368–3373.
[30] Y. Wu, A. Shi, Y. Li, H. Zeng, X. Chen, J. Wu, X. Fan, A near-infrared xanthene fluorescence probe for monitoring peroxynitrite in living cells and mouse inflammation model, Analyst 143 (2018) 5512–5519.
[31] R. Yuan, Y. Ma, J. Du, F. Meng, J. Guo, M. Hong, Q. Yue, X. Li, C. Li, A novel highly selective near-infrared and naked-eye fluorescence probe for imaging peroxynitrite, Anal. Methods 11 (2019) 1522–1529.
[32] J. Qian, D. Gong, J. Ru, Y. Guo, T. Cao, W. Liu, W. Qin, H. Guo, A naphthalimide-based lysosome-targeting fluorescent probe for the selective detection and imaging of endogenous peroxynitrite in living cells, Anal. Bioanal. Chem. 411 (2019) 3929–3939.
[33] S.V. Mulay, Y. Kim, K.-J. Lee, T. Yudhistira, H.-S. Park, D.G. Churchill, A fluorogenic and red-shifted diphenyl phosphinate-based probe for selective peroxynitrite detection as demonstrated in fixed cells, New J. Chem. 41 (2017) 11934–11940.
[34] Y. Shen, L. Dai, Y. Zhang, H. Li, Y. Chen, C. Zhang, A novel pyridinium-based fluorescent probe for ratiometric detection of peroxynitrite in mitochondria, Spectrochim. Acta A 228 (2020), 117762.
[35] D. Yang, H.-L. Wang, Z.-N. Sun, N.-W. Chung, J.-G. Shen, A highly selective fluorescent probe for the detection and imaging of peroxynitrite in living cells, J. Am. Chem. Soc. 128 (2006) 6004–6005.
[36] F. Yu, P. Li, G. Li, G. Zhao, T. Chu, K. Han, A Near-IR reversible fluorescent probe modulated by selenium for monitoring peroxynitrite and imaging in living cells, J. Am. Chem. Soc. 133 (2011) 11030–11033.
[37] T. Peng, N.-K. Wong, X. Chen, Y.-K. Chan, D.H. Ho, Z. Sun, J.J. Hu, J. Shen, H. El-Nezami, D. Yang, Molecular imaging of peroxynitrite with HKGreen-4 in live cells and tissues, J. Am. Chem. Soc. 136 (2014) 11728–11734.
[38] X. Li, R. Tao, L. Hong, J. Cheng, Q. Jiang, Y. Lu, M. Liao, W. Ye, N. Lu, F. Han, Y. Hu, Visualizing peroxynitrite fluxes in endothelial cells reveals the dynamic progression of brain vascular injury, J. Am. Chem. Soc. 137 (2015) 12296–12303.
[39] C. Liu, C. Shao, H. Wu, B. Guo, B. Zhu, X. Zhang, A fast-response, highly sensitive and selective fluorescent probe for the ratiometric imaging of hydrogen peroxide with a 100 nm red-shifted emission, RSC Adv. 4 (2014) 16055–16061.
[40] Z. Wang, L. Wu, Y. Wang, M. Zhang, Z. Zhao, C. Liu, Q. Duan, P. Jia, B. Zhu, A highly selective and ultrasensitive ratiometric fluorescent probe for peroxynitrite and its two-photon bioimaging applications, Anal. Chim. Acta 1049 (2019) 219–225.
[41] Z. Li, S. Huang, Y. He, Q. Duan, G. Zheng, Y. Jiang, L. Cai, Y. Jia, H. Zhang, D. Ho, AND logic gate based fluorescence probe for simultaneous detection of peroxynitrite and hypochlorous acid, Spectrochim. Acta A 230 (2020), 118073.
[42] Y. Shen, M. Li, M. Yang, Y. Zhang, H. Li, X. Zhang, A specific AIE and ESIPT fluorescent probe for peroxynitrite detection and imaging in living cells, Spectrochim. Acta A 222 (2019), 117230.
[43] D. Liu, Y. Lv, M. Chen, D. Cheng, Z. Song, L. Yuan, X. Zhang, A long wavelength emission two-photon fluorescent probe for highly selective detection of cysteine in living cells and an inflamed mouse model, J. Mater. Chem. B 7 (2019) 3970–3975.
[44] D. Cheng, Y. Pan, L. Wang, Z. Zeng, L. Yuan, X. Zhang, Y.-T. Chang, Selective visualization of the endogenous peroxynitrite in an inflamed mouse model by a mitochondria-targetable two-photon ratiometric fluorescent probe, J. Am. Chem. Soc. 139 (2017) 285–292.
[45] Y. Cheng, J. Dai, C. Sun, R. Liu, T. Zhai, X. Lou, F. Xia, An intracellular H_2O_2-responsive AIEgen for the peroxidase-mediated selective imaging and inhibition of inflammatory cells, Angew. Chem. Int. Ed. 57 (2018) 3123–3127.
[46] J. Zhang, X. Ji, J. Zhou, Z. Chen, X. Dong, W. Zhao, Pyridinium substituted BODIPY as NIR fluorescent probe for simultaneous sensing of hydrogen sulphide/glutathione and cysteine/homocysteine, Sens. Actuators, B 257 (2018) 1076–1082.
[47] J. Gao, Y. Tao, J. Zhang, N. Wang, X. Ji, J. He, Y. Si, W. Zhao, Development of lysosome-targeted fluorescent probes for Cys by regulating the boron-dipyrromethene (BODIPY) molecular structure, Chem. Eur. J. 25 (2019) 11246–11256.
[48] N. Wang, M. Chen, J. Gao, X. Ji, J. He, J. Zhang, W. Zhao, A series of BODIPY-based probes for the detection of cysteine and homocysteine in living cells, Talanta 195 (2019) 281–289.
[49] J. Zhang, N. Wang, X. Ji, Y. Tao, J. Wang, W. Zhao, BODIPY-based fluorescent probes for biothiols, Chem. Eur. J. 26 (2020) 4172–4192.
[50] X. Wang, Y. Tao, J. Zhang, M. Chen, N. Wang, X. Ji, W. Zhao, Selective detection and visualization of exogenous/endogenous hypochlorous acid in living cells using a BODIPY-based red-emitting fluorescent probe, Chem. Asian J. 15 (2020) 770–774.
[51] X. Ji, N. Wang, J. Zhang, S. Xu, Y. Si, W. Zhao, Meso-pyridinium substituted BODIPY dyes as mitochondria-targeted probes for the detection of cysteine in living cells and in vivo, Dyes Pigments 187 (2021), 109089.
[52] Z. Li, X. Li, X. Gao, Y. Zhang, W. Shi, H. Ma, Nitroreductase detection and hypoxic tumor cell imaging by a designed sensitive and selective fluorescent probe, 7-[(5-Nitrofuran-2-yl) methoxy]-3H-phenoxazin-3-one, Anal. Chem. 85 (2013) 3926–3932.
[53] W. Gao, B. Xing, R.Y. Tsien, J. Rao, Novel fluorogenic substrates for imaging β-lactamase gene expression, J. Am. Chem. Soc. 125 (2003) 11146–11147.
[54] M.L. Odyniec, A.C. Sedgwick, A.H. Swan, M. Weber, T.M.S. Tang, J.E. Gardiner, M. Zhang, Y. Jiang, G. Kociok-Kohn, R.B.P. Elmes, S.D. Bull, X. He, T.D. James, 'AND'-based fluorescence scaffold for the detection of ROS/RNS and a second analyte, Chem. Commun. 54 (2018) 8466–8469.
[55] J. Wang, Y. Men, L. Niu, Y. Luo, J. Zhang, W. Zhao, J. Wang, A reaction-based fluorescent probe for imaging of native hypochlorous acid, Chem. Asian J. 14 (2019) 3893–3897.
[56] J.J. Morsby, M. Dharmarwardana, H. McGarraugh, B.D. Smith, Supramolecular optimization of the visual contrast for colorimetric indicator assays that release resorufin dye, Chem. Commun. 56 (2020) 9296–9299.
[57] R.A. Hankins, S.I. Suarez, M.A. Kalk, N.M. Green, M.N. Harty, J.C. Lukesh III, An innovative hydrogen peroxide-sensing scaffold and insight towards its potential as an ROS-activated persulfide donor, Angew. Chem. Int. Ed. 59 (2020) 22238–22245.
[58] A.K. Yadav, C.J. Reinhardt, A.S. Arango, H.C. Huff, L. Dong, M.G. Malkowski, A. Das, E. Tajkhorshid, J. Chan, An activity-based sensing approach for the detection of cyclooxygenase-2 in live cells, Angew. Chem. Int. Ed. 59 (2020) 3307–3314.
[59] Z. L, H. M, Progress in resorufin-based spectroscopic probes, Imaging Sci. Photochem. 32 (2014) 60−68.
[60] Y. Zhang, D. Ma, Selective detection of peroxynitrite in living cells by a near-infrared diphenyl phosphinate-based dicyanoisophorone probe, Spectrochim. Acta A 244 (2021), 118890.
[61] F. Yu, P. Li, B. Wang, K. Han, Highly selective fluorescent probe based on hydroxylation of phenylboronic acid pinacol ester for detection of tyrosinase in cells chromogenic and fluorogenic signaling of sulfite by selective deprotection of resorufin levulinate, J. Am. Chem. Soc.. 135 (2013) 7674–7680.
[62] J. Li, L. Chen, Q. Wang, H. Liu, X. Hu, L. Yuan, X. Zhang, A bioluminescent probe for imaging endogenous peroxynitrite in living cells and mice, Anal. Chem. 90 (2018) 4167–4173.